

Metamaterial-based wearable flexible elliptical UWB antenna for WBAN and breast imaging applications

Cite as: AIP Advances **11**, 015128 (2021); <https://doi.org/10.1063/5.0037232>

Submitted: 18 November 2020 • Accepted: 07 December 2020 • Published Online: 14 January 2021

 Adam R. H. Alhawari,  A. H. M. Almawgani,  Ayman Taher Hindi, et al.

COLLECTIONS

Paper published as part of the special topic on [Materials Science](#)



View Online



Export Citation



CrossMark

ARTICLES YOU MAY BE INTERESTED IN

[Electronic bandgap miniaturized UWB antenna for near-field microwave investigation of skin](#)

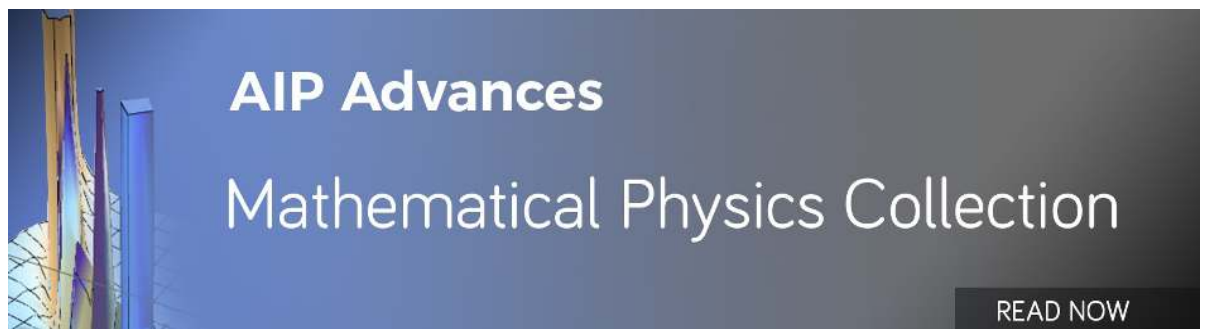
AIP Advances **11**, 035228 (2021); <https://doi.org/10.1063/5.0030126>

[Near-field and far-field investigation of miniaturized UWB antenna for imaging of wood](#)

AIP Advances **9**, 035232 (2019); <https://doi.org/10.1063/1.5081762>

[Dielectric properties of complete oil palm trunk sample \(healthy and unhealthy\)](#)

AIP Advances **9**, 075314 (2019); <https://doi.org/10.1063/1.5094459>



AIP Advances
Mathematical Physics Collection

READ NOW

Metamaterial-based wearable flexible elliptical UWB antenna for WBAN and breast imaging applications

Cite as: AIP Advances 11, 015128 (2021); doi: 10.1063/5.0037232

Submitted: 18 November 2020 • Accepted: 7 December 2020 •

Published Online: 14 January 2021



View Online



Export Citation



CrossMark

Adam R. H. Alhawari,^{1,a)}  A. H. M. Almawgani,^{1,b)}  Ayman Taher Hindi,^{1,c)}  Hisham Alghamdi,^{1,} 
and Tale Saeidi² 

AFFILIATIONS

¹Electrical Engineering Department, College of Engineering, Najran University, Najran, Kingdom of Saudi Arabia

²Electrical and Electronic Engineering Department of Universiti Teknologi PETRONAS, 32610 Bandar Seri Iskandar, Perak, Malaysia

^{a)} Author to whom correspondence should be addressed: aralhawari@nu.edu.sa

^{b)} ahalmawgani@nu.edu.sa

^{c)} athindi@nu.edu.sa

^{d)} hg@nu.edu.sa

ABSTRACT

This paper presents a metamaterial-based flexible wearable ultra-wideband (UWB) antenna for breast imaging and wireless body area network (WBAN) applications. The wearable antenna is required to be a planar and low-profile structure using flexible materials. The proposed antenna comprises two layers of denim ($10 \times 10 \text{ mm}^2$) and felt ($10 \times 15 \text{ mm}^2$). The antenna was integrated with six metamaterial unit cells using a modified grain rice shape within a split ring resonator to enhance the bandwidth, gain, and directivity and reduce the specific absorption rate value to less than 2 W/kg . The proposed antenna operates within a broad bandwidth range (6.5 GHz–35 GHz) with the maximum gain and directivity of 8.85 dBi and 10 dBi, respectively, and a radiation efficiency of more than 70% over its operating frequency band. The results verified good agreement between the simulation and measurement of the proposed technique in detecting an existing tumor with a diameter of 4 mm from any location inside the breast. The results convincingly proved the capability of the proposed wearable UWB antenna system for both WBAN and breast imaging applications.

© 2021 Author(s). All article content, except where otherwise noted, is licensed under a Creative Commons Attribution (CC BY) license (<http://creativecommons.org/licenses/by/4.0/>). <https://doi.org/10.1063/5.0037232>

I. INTRODUCTION

Lately, wearable and flexible antennas have been produced for various applications, such as communication and embedded smart systems and health monitoring purposes. The recent rapid development of wearable wireless devices and wireless body area network (WBAN) has attracted the attention of many researchers. The current hectic situation of the hospitals and their standard operational procedures (SOP) due to the COVID-19 pandemic challenges had made healthcare practitioners aware of the need to increase contactless medical procedures to avoid the spread of the infection. If there is innovation to avoid contact with patients for safety reason, it is better where it is possible for the staff nurse to follow up vital signs remotely.¹ Apart from that, the healthcare providers are

searching for ways to outsource medical care to overcome intensified workload.² This is a golden chance to promote further usage of WBAN within the medical care sphere. It is useful for continuous monitoring of vital signs related to the bodies, as shown in Fig. 1.³ Most of the invented on-body applications are small, lightweight, yet robust, and stretchable antennas that can easily maintain a reliable and high-performance communication.⁴ Usually, the WBAN systems are worn on body, so they are prone to bending or contact with skin directly or be affected with body interaction, which may degrade the antenna radiation characteristics and detune its impedance matching. These possibilities will reduce the system efficiency and throughput signal. Moreover, devices that need to be wrapped or attached to any body parts may be influenced by movement and physiological changes such as respiration and sweating,

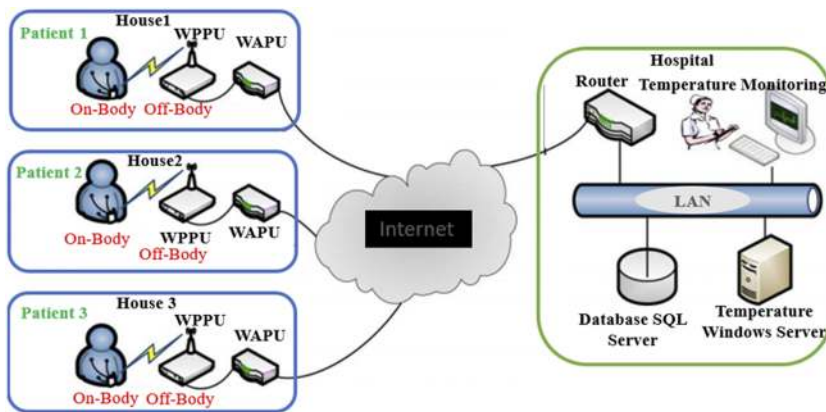


FIG. 1. A general architecture of the monitoring system: WPPU (Wireless Patient Portable Unit) and WAPU (Wireless-Access Point Unit).³

and temperature changes may create the WBAN channels that are prone to time-varying received characteristics. Therefore, in order to reduce the aforementioned problems, this work proposes a small size and flexible planar antenna at a low cost as it can easily be integrated into on-body electronic systems.^{5–10} The wearable antennas and WBAN system offer better solution for the breast cancer patients because they can do their check up from home without going to the hospital especially during the COVID-19 pandemic where the social distance is required by SOP, as well as in the absence of the pandemic to avoid mixing with other sick people due to their compromised immune system especially prior and post treatments.

The antenna is the key component within a WBAN system and it is an important part of a wearable monitoring system.¹¹ The integration of wearable antennas with various electronic systems requires attention to reduce the on-body detuning. The antenna detuning effects depend on the antenna form factor, its distance from the skin, and the body shape. The detuning effects may be reduced using different structures including defected or truncated structures. Flexible textile antennas are good candidates for the WBAN systems due to their flexibility and ease of integration with the textile materials.⁸ Numerous single, dual, and multiband flexible wearable antennas showing a good performance have been proposed in the literature.^{12–23} As the demand increased for the usage of mobile devices and unlicensed bands, more reliable and faster networks are needed. Therefore, the concept of the smart towns, smart surface, and internet of things (IoT) came to mind to overcome various infrastructure issues. One of the alternatives is to combine wireless technology with other technologies such as artificial intelligence; for example, the initiation of the new generation communication at the free operating frequency bands.

Along with the rise of IoT and other massive-machine type communications (MTC), the 5G showed an increment in the capacity as compared to the 4G networks.²⁴ The new applications such as multi-way virtual meeting, virtual and augmented reality (VAR) and their requirements, remote hospital operations, and smart building and surfaces depicted that low frequency 5G bands will not be able to satisfy the demands from the massive users from these applications and a solution as higher as 5G bands and 6G should be introduced to replace them.^{25–29} Only then, it can be helpful to fulfill the combination of remote operation in hospitals, medical imaging, and sensing devices.^{30–33} Besides, based on the consumption factor theory, the

power efficiency increases with bandwidth (BW), and more efficient energy is achievable when the higher band is utilized. Furthermore, when an antenna shows high gain and directivity while having small physical dimensions, the attenuations can be overcome, and it offers more array integration, consuming less printing area.³⁴

The wearable antennas should be designed carefully not to affect the human body when they are worn. One of the parameters that should be taken care of while designing a wearable antenna is having low Specific Absorption Rate (SAR; should be less than 2). Having a complete ground acting as a shield, it is helpful to keep the SAR low. Apart from that the metasurface, electronic bandgap (EBG) and integrating a layer of metamaterial (MTM) can keep the SAR value in the acceptable range. Various techniques such as metasurface and large intelligent surfaces (LIS) were used to obtain high gain and directive antenna.^{35–37} An ultra-wideband (UWB) antenna was loaded with metamaterial (MTM) for the C-band applications.^{38,39}

In addition to that, wearable UWB antennas were designed to operate at 3.1 GHz–11.3 GHz,⁴⁰ 2.9 GHz–11 GHz,⁴¹ 3 GHz–12 GHz,⁴² and 2.7 GHz–10.26 GHz.⁴³ A textile substrate material with a fractal patch was designed to resonate in the band of 1.4 GHz–20 GHz to be applicable for WBAN application.⁴⁴ A novel wearable textile antenna with dimensions of $51 \times 45 \text{ mm}^2$ was designed for ISM application.⁴⁵ A flexible planar quasi-Yagi UWB antenna was designed for WBAN with the BW of 7.4 GHz and dimensions of $34 \times 30 \text{ mm}^2$.⁴⁶ A more flexible UWB antenna designed for communication, WBAN, and breast cancer detection applications was presented in Refs. 47–49.

II. ANTENNA DESIGN

The designed prototype and the antenna dimensions for each part are shown in Fig. 2 and Table I, respectively. First, a conventional elliptical patch antenna was designed and fed through a transmission line on a denim substrate with a dielectric constant of 1.2 and a thickness of 0.7 mm. The initial dimensions of the antenna substrate are defined by applying the microstrip antenna equations presented in Ref. 50.

After obtaining the result of the conventional antenna, some stop bands were noticed at the working BW. Consequently, the surface current distribution of the antenna should be examined at the

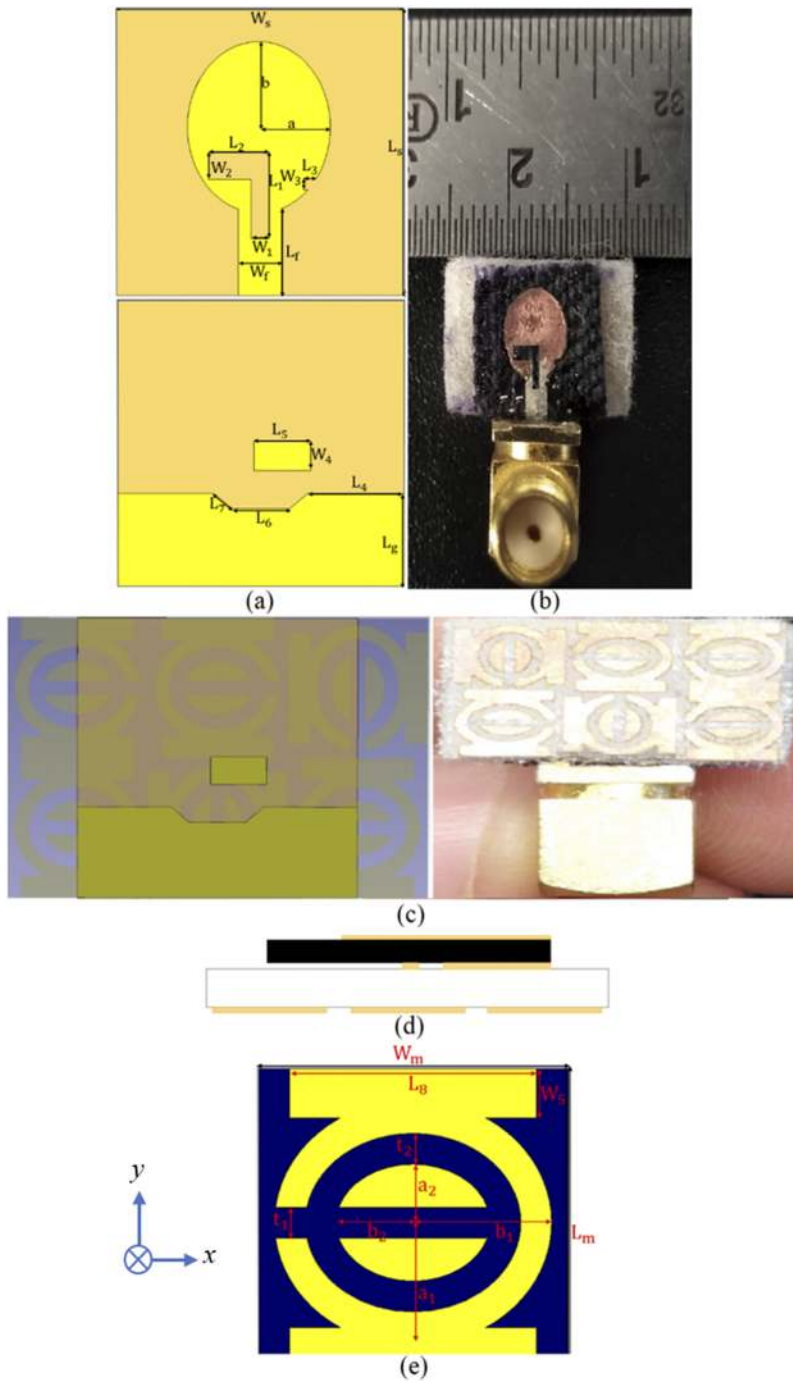


FIG. 2. The simulated and fabricated prototype of the antenna: (a) simulated UWB antenna, (b) fabricated antenna with MTM, (c) simulated antenna with MTM arrays, (d) side view, and (e) MTM unit cell.

operating frequency. Figure 3 depicts the surface current distribution at the lower end and higher end of the antenna BW, and the stop bands occurred in the BW. The surface current is stronger around the transmission line and the patch at the operating frequency, which is helpful in the designing process technique. After the surface current distribution was checked, the ground was cut in the middle, and then, it was chamfered to enhance the BW of

the antenna and remove the stop band that occurred at 15 GHz. However, the BW was extended at the higher band up to 35 GHz by cutting the ground, but some stop bands were still detected and then removed. Afterward, the elliptical patch is etched using an L-shaped slot to eliminate the stop band around 25 GHz and change the polarization to circular. Moreover, another rectangular slot is cut for further stop band removal and improves the reflection coefficient

TABLE I. Antenna dimensions.

| Parameters | Dimensions (mm) | Parameters | Dimensions (mm) |
|------------|-----------------|------------|-----------------|
| L_s | 10 | W_1 | 0.625 |
| L_g | 5 | W_2 | 0.925 |
| L_f | 3 | W_3 | 0.4 |
| L_1 | 3 | W_4 | 1 |
| L_2 | 1.2 | W_5 | 0.8 |
| L_3 | 0.45 | W_m | 5 |
| L_4 | 3.35 | t_1 | 0.5 |
| L_5 | 2 | t_2 | 0.5 |
| L_6 | 2 | a | 2.5 |
| L_7 | 0.85 | a_1 | 1.75 |
| L_8 | 4 | a_2 | 1 |
| L_m | 5 | b | 3 |
| W_s | 10 | b_1 | 2.25 |
| W_f | 1.5 | b_2 | 1.25 |

level at a higher band. In addition to that, the antenna is loaded using a small stub next to the ground to improve the reflection coefficient level around 33 GHz and remove the stop bands at 25 GHz–28 GHz. However, the surface current distribution around the slot cut from the patch indicates more density at 33 GHz and 35 GHz stop bands.

Table I represents the antenna's designed parameters and dimensions. Among all these parameters, some of them affect the reflection coefficient result and the operating BW more dramatically than others when they were investigated in the simulation. For instance, the elliptical patch dimensions (a and b), the transmission line's width and length (L_f and W_f), the ground length (L_g), and the space between the ground and the stub located at the back play more important roles in matching and the reflection coefficient result as compared to the other parameters. Furthermore, L_f and b affect the BW when shifting it to a lower or higher band, and a and W_f proportionally affect BW and the input impedance, respectively. Besides, L_g affects the BW as well. As mentioned above, at a higher frequency such as 5G, an antenna with a highly directive beam, high gain, and high radiation efficiency is required. Therefore, a metamaterial (MTM) structure (a combination of ϵ -negative and μ -negative groups) was integrated to enhance the overall performance of the proposed antenna as that method is capable of obtaining a narrower -3 dB beam, more directivity, enhanced gain, higher radiation efficiency, and extended BW.

Metamaterial structures are assumed as patterned and periodic planar structures are utilized to obtain broad BW, low-profile and stack structure, and higher directive gain. Figure 1(e) shows the proposed MTM unit cell structure. The initial MTM unit was designed based on a split ring resonator (SRR) containing a bigger elliptical SRR and smaller modified grain rice shape within the bigger one.⁵¹ The grain rice shape is selected due to its excellent electromagnetic performances such as anisotropy control, vast BW, and loss in metal.⁵² The SRR is a structure that resonates magnetically, and it is affected by the perpendicular magnetic field to create magnetic permeability.^{53,54} On the other hand, the gaps (splits) are usually added to the design to introduce capacitance and to control the resonant

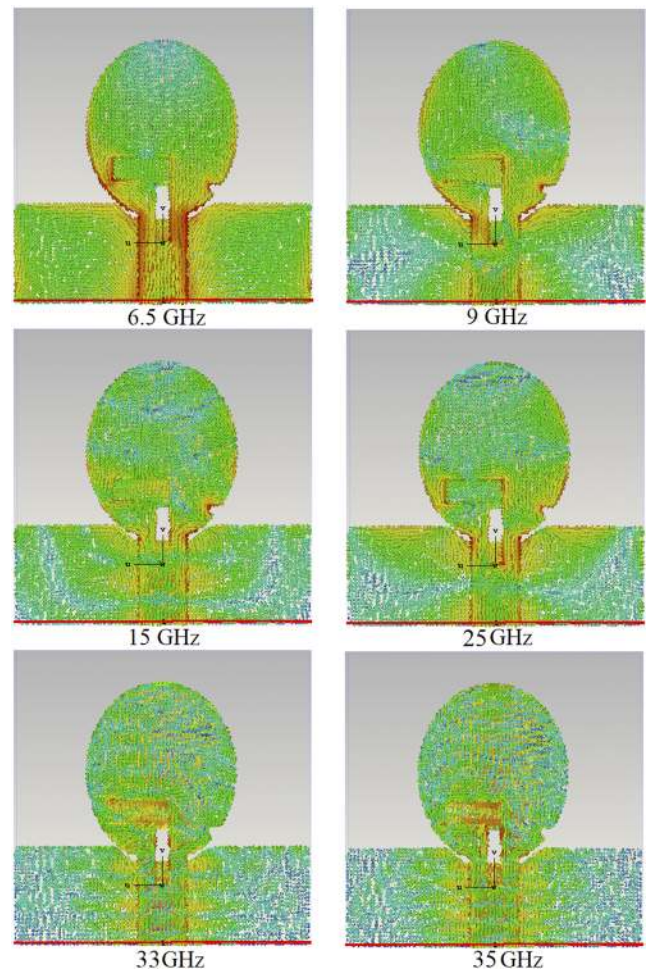


FIG. 3. Single antenna's surface current distribution without the layer of MTM arrays.

specification of the structure. In addition, the grain rice shape is cut using a gap to increase the series capacitance of the SRR and reduce the coupling between the inner and outer of the ring and produce a broad forward-wave passband.⁵¹ Afterward, two capacitive-loaded strips (CLSs) are added to the structure to make the resonant profile of the structure within the UWB range. CLS structures act like an electric dipole and an electric wire.⁵⁵ Besides, the combination of the structures introduces a simultaneous electric (\mathbf{E}) and magnetic (\mathbf{H}) fields and the CLSs give a parallel \mathbf{E} -field.

The MTM unit cell shown in Fig. 1(e) was designed on a flexible textile "felt" substrate with a dielectric constant of 1.4 and a thickness of 1.5 mm. The finite-difference time domain (FDTD) was utilized in Computer Simulation Technology (CST) Microwave studio to calculate and simulate the S-parameters. Therefore, two waveguide ports and magnetic/electric boundaries are set around the MTM structure. Afterward, both perfect magnetic and electric conductors are determined toward the x -axis and y -axis, respectively. Besides, the z -axis is considered as open space, and then,

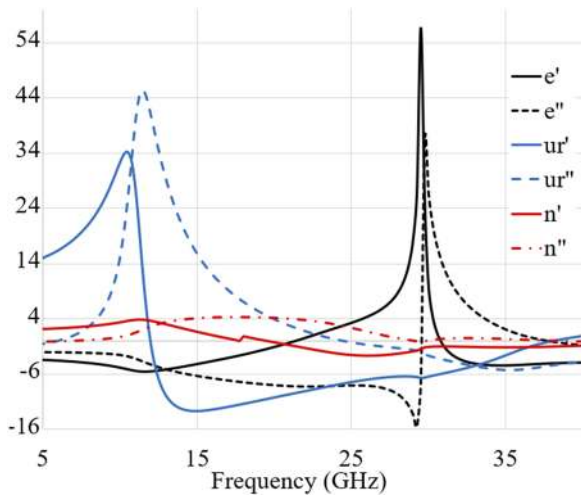


FIG. 4. The retrieved effective parameters of the MTM unit cell.

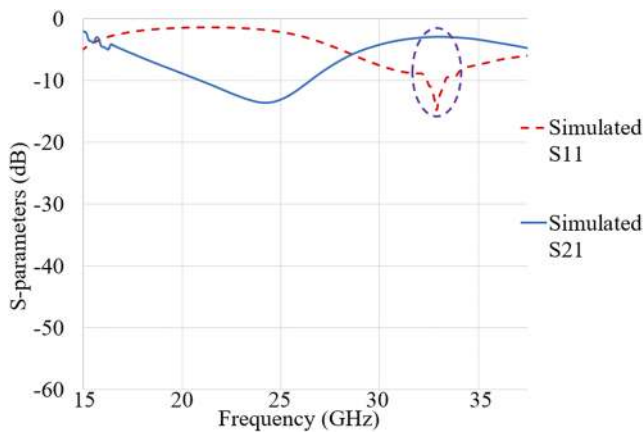


FIG. 5. Simulated reflection and transmission coefficient results of the MTM unit cell.

the MTM structure is fed in this direction. In fact, the structure is designed to have a negative index at the stop bands that occurred in the antenna’s working BW: both at the higher end of the working BW and the lower end. In addition, the Nicolson–Ross–Weir (NRW) method reported in Ref. 56 was performed to investigate the electromagnetic specifications of the proposed MTM unit cell to calculate and extract the permittivity (ϵ), permeability (μ), and refractive index (n) from the simulated reflection and transmission coefficient results, as shown Figs. 4 and 5. The operating BW range

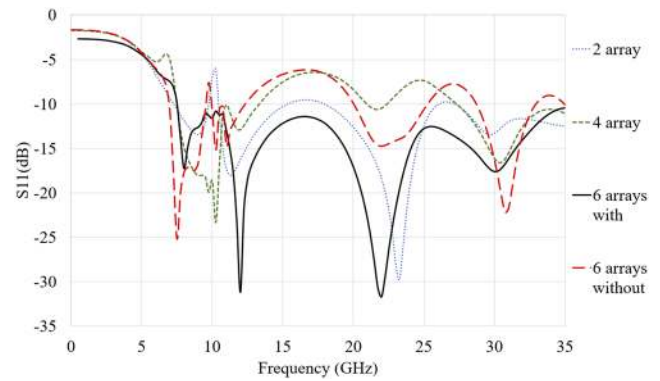


FIG. 6. Reflection coefficient results for different numbers of MTM arrays.

of ϵ , μ , and n is summarized in Table II. It was based on what presented in Figs. 4 and 5. As illustrated in Fig. 5, the transmission coefficient result shows a peak at 33 GHz. After investigation of the proposed MTM structure in terms of the negative index, six arrays of the proposed MTM are integrated with the antenna to improve the antenna performance in terms of gain, directivity, radiation efficiency, and impedance matching. Besides, these six arrays rotate with 90° difference starting from the second array to the fifth one, as shown in Fig. 1(c).

III. RESULTS AND DISCUSSION

The proposed MTM-based UWB antenna is simulated, fabricated, and measured. The performance of the proposed antenna was evaluated in terms of the reflection coefficient with different numbers of the MTM arrays, as shown in Fig. 6. The result shows that a broad BW was achievable (below -10 dB) when the array numbers were enhanced, and stop bands were eliminated. Also, when six MTM arrays were utilized and integrated with the antenna, better results were obtained, as revealed in Fig. 6. Interestingly, the performance of the antenna had improved further when the MTM arrays were rotated by 90° . Additionally, the reflection coefficient results were analyzed and compared when integrated with six MTM arrays and without MTM arrays, as presented in Figs. 6 and 7. Essentially, the analysis was preceded by an investigation on the effects of the array numbers on the performance of the antenna, as illustrated in Fig. 6.

Figure 7 illustrates the return loss results of the proposed antenna with six MTM arrays along with 90° rotation and without MTM arrays. The overall results discovered that the antenna with six MTM arrays along with 90° rotation performs better compared to the other considerations when simulated. Moreover, the operating BW range was extended to both lower and higher ends of the BW. For instance, the lower end of the BW is extended to almost

TABLE II. Negative index frequency regions of the MTM unit cell.

| Parameters | Permittivity (ϵ) | Permeability (μ) | Refractive index (n) |
|--------------------|-----------------------------|------------------------|--------------------------|
| Operating BW (GHz) | 3–22, 32–40 | 12.5–39.5 | 19.5–40 |

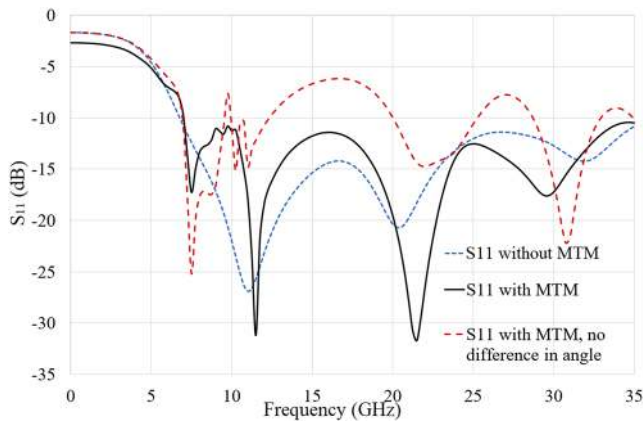


FIG. 7. Reflection coefficient results when the arrays are rotated by 90° .

2 GHz, and the stop bands around 25 GHz and 34 GHz were removed and became passbands.

Figure 8 depicts the simulated and measured radiation pattern of the proposed antenna integrated with the MTM arrays (right-hand side) and without MTM arrays (left-hand side). As the results revealed, the narrower -3 dB beam and significant enhancement in the directivity are obtainable only when the antenna is integrated with the MTM arrays. Then, the measured radiation pattern represents good agreement with the simulated one. However, the measurement of the radiation patterns for frequencies more than 20 GHz (the maximum vector network analyzer frequency) was unable to be performed due to equipment shortage in the laboratory of researchers. It is worthwhile to mention that in order to solder the antenna to the SubMiniature version A (SMA) port, the hot soldering method is used for the copper conductor. Next, a conductive epoxy glue was used to paste it to the denim substrate (the SMA port was used to measure until 27 GHz, while another connector model No. 1892-04A-5 from Southwest Microwave was used for higher frequencies).

The simulated and measured results of the gain and efficiency of the proposed antenna are presented in Fig. 9. It evidently demonstrates that both simulated and measured results of gain and radiation efficiency are in competent agreement and follow the same tendency. Moreover, the gain of the antenna has been greatly improved by the MTM arrays about 5.5 dBi within its operating frequency band compared to the one without MTM structure. Similarly, the radiation efficiency has been enhanced by about 10% when the antenna is integrated with MTM arrays. Overall, the proposed antenna shows a maximum gain of 8.85 dBi and a maximum radiation efficiency of 94% at the frequency of 30 GHz. Besides, the result shows that the radiation efficiency is higher than 70% from 10 GHz to 35 GHz. Table III represents the performance of the proposed antenna compared with recent similar works in terms of gain, bandwidth, and dimensions. Favorably, as it is observable from Table III, the proposed antenna has a smaller size and high gain within its frequency bandwidth compared to the other antennas presented in Table III. The results verified the capability of the proposed technique applied in this work to improve the overall performance of its antenna to suit both WBAN and breast imaging applications.

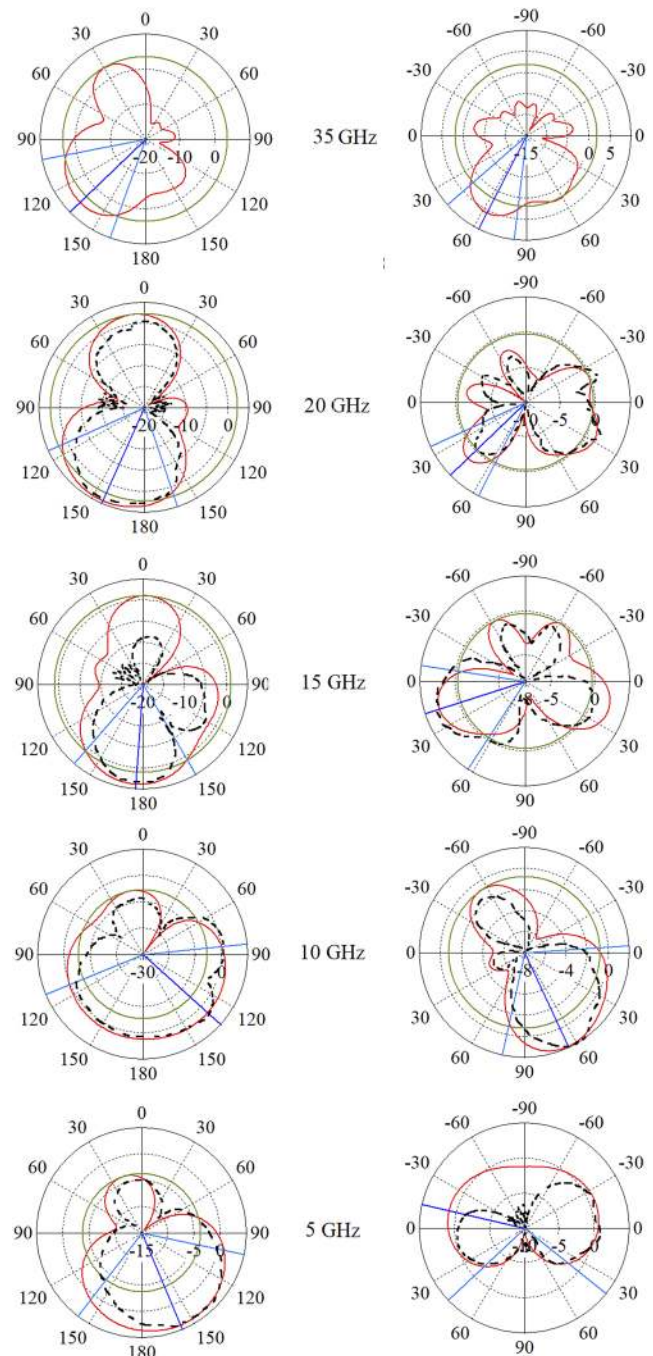


FIG. 8. The off-body radiation pattern of the antenna (right-hand side—with MTM arrays, left-hand side—without MTM arrays, solid line—simulated E-plane, and dashed line—measured E-plane).

After simulating and measuring the antenna performance in air (off-body), it was measured on the body: on the chest and the arm to observe how much the results would alter after changing the environment from the arm to the chest (Fig. 10). The simulated

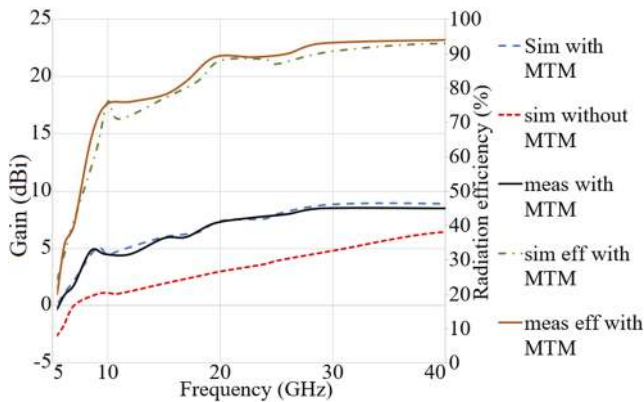


FIG. 9. Simulated and measured result of gain and efficiency.

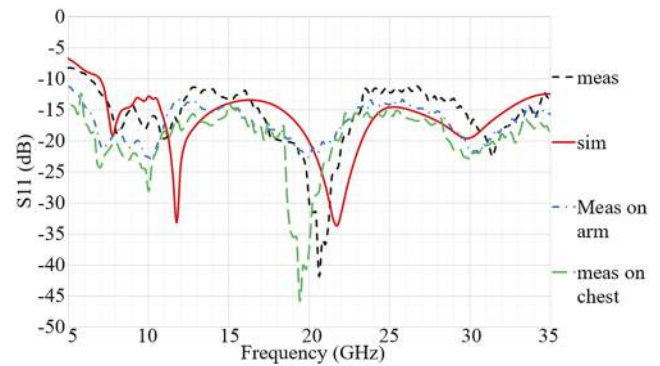


FIG. 11. Simulated and measured reflection coefficient result of the antenna with MTM.

TABLE III. Antenna performance comparison.

| References | Dimensions (mm ²) | BW (GHz) | Max gain (dBi) |
|------------|-------------------------------|----------|----------------|
| 57 | 20 × 20 | 2–18 | >−2.65 |
| 58 | 28.6 × 28.6 | 2–27 | ... |
| 59 | 16 × 16 | 26–40 | 7.44 |
| 60 | 50 × 40 | 2.2 – 25 | 4.5 |
| 61 | 26 × 16 | 18–44 | 1.45 |
| 62 | 50.8 × 62 | 1.3–20 | 10 |
| Proposed | 10 × 15 | 6.5–35 | 8.85 |

and measured reflection coefficient results of the antenna with MTM arrays on body conditions are shown in Fig. 11. Finally, the simulated and measured results empirically yielded good agreement. All the four resonating poles were achieved in the measurement with a slight shift only being observed when it contacts the arm and the chest. Nonetheless, the reflection coefficient level was reduced by almost −5 dB compared to the simulation results. Besides, the reflection coefficient results on the chest were shifted down more than on the arm. It might be due to different composition of the skin layers and structures whereby the skin maybe is thicker around the chest as compared to the arm.^{63,64}

Another important factor that should be considered for flexible wearable antennas is the SAR value. Based on the principles, it should be less than 2 W/kg for both standards of 1 g and 10 g. Figure 12 and Table IV present the result of SAR values on the layers of skin, breast fat, muscle, and bone at the working BW of the proposed antenna. The results showed that the SAR values met the standard requirements mentioned.

A. Antenna investigations in breast environment

Before discussing about the results, it better to show how the antenna of the UWB operates in both time and frequency domains. Typically, narrow-band antennas and propagation are described in the frequency domain. Usually, the characteristic parameters are assumed to be constant over a few percent bandwidth. In this case, the frequency-dependent characteristics of the antennas and the frequency-dependent behavior of the channel for UWB systems should be considered. In addition, as the UWB systems are often realized in an impulse-based technology, therefore, the time-domain effects and properties should be discovered together for consideration along with the previously mentioned characteristics. Speaking on the ground of the frequency-domain description, it is assumed that the transmitter antenna is excited with a continuous wave. Meanwhile, the time-domain description assumes that the transmit antenna is excited with an impulse signal with the frequency f .



FIG. 10. The on-body measurement setup on (a) the chest and (b) the arm.

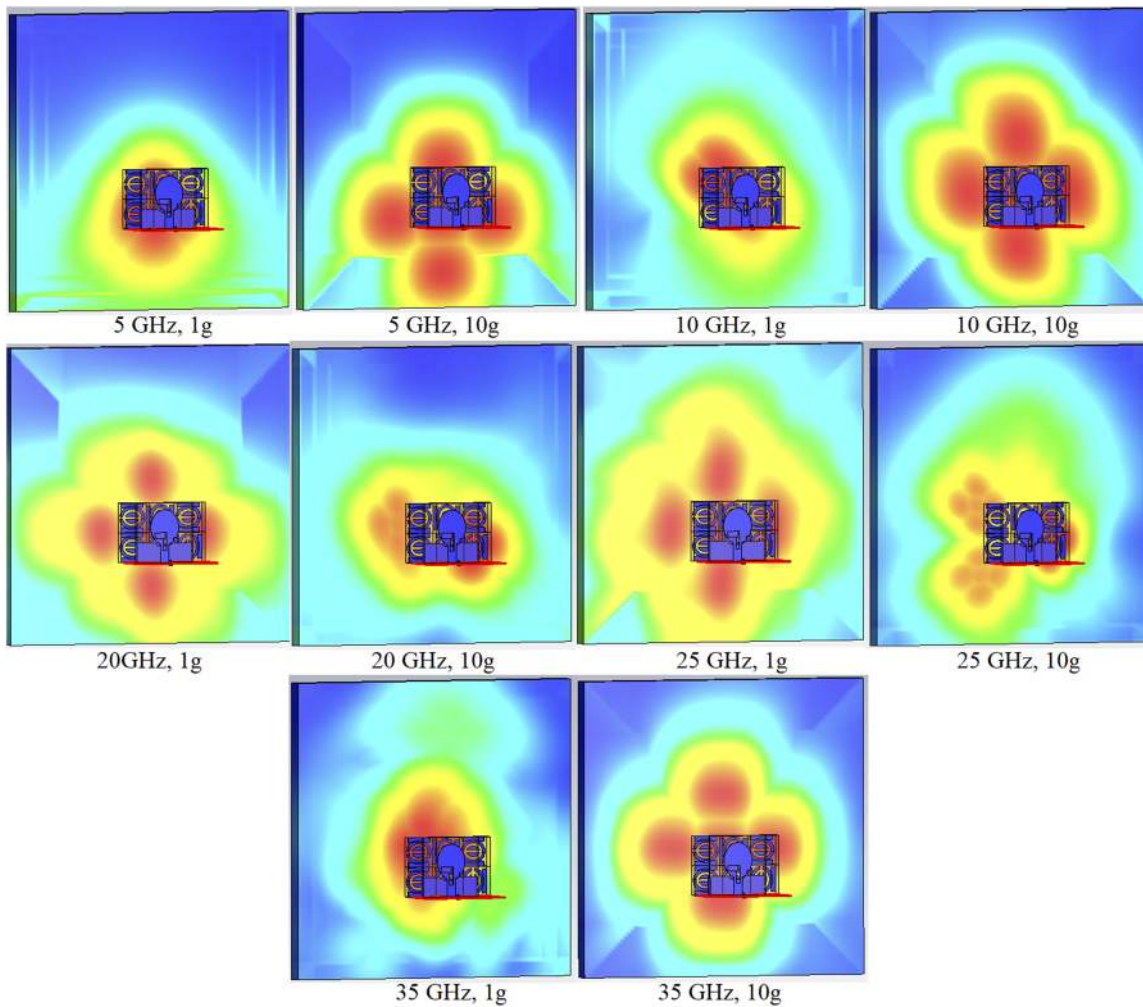


FIG. 12. SAR variation on body for both 1 g and 10 g at different frequencies.

Accordingly, the frequency domain assumes that the antenna transfer functions represent a two-dimensional vector with two orthogonal polarization components, but in the time domain, the antenna transient response becomes more adequate for the description of impulse systems. The antenna transient response mainly depends on time, together with the angles of departures and arrivals, and polarization. Figure 13 shows the procedure of sending and receiving a

pulse between two UWB antennas in the time domain [both the transmitted pulse and output voltage are of the same scale, as the vertical axis is the amplitude of the signal and the horizontal axis is the time in nanoseconds (ns)].

TABLE IV. SAR values at different frequencies.

| Frequency (GHz) | 1 g | 10 g |
|-----------------|-------|-------|
| 5 | 0.355 | 0.164 |
| 10 | 1.98 | 1.14 |
| 20 | 1.11 | 0.536 |
| 25 | 0.52 | 0.276 |
| 35 | 2.01 | 1.18 |

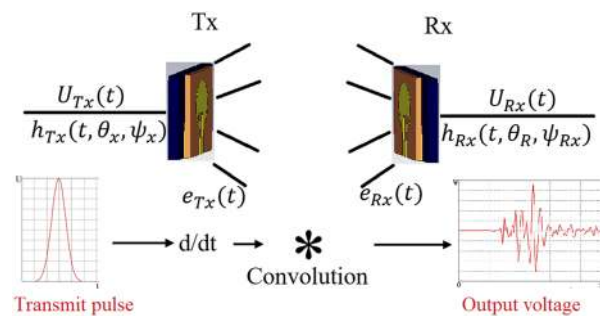


FIG. 13. UWB antenna transceiver system in the time domain.

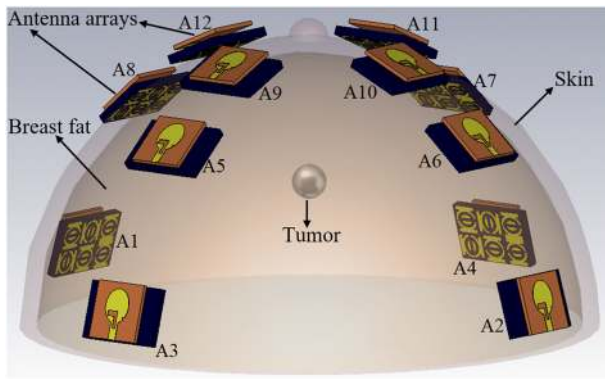


FIG. 14. The simulation setup with antenna arrays and breast model.

Prior to constructing an image of a tumor in the breast using the simulation data, some important parameters that can affect the imaging processes are investigated and evaluated. Based on the simulation setup shown in Fig. 14, 12 arrays of the proposed antenna are located around the breast to investigate the impacts of these arrays on each other. One of the primary parameters that should be considered is the recipient signals from different arrays. Both the recipient signals and their delays are utilized in the analysis in Sec. III B to reconstruct the image of the tumor. Figure 15 indicates the recipient signals from different arrays. As illustrated below, the array (A1) in the investigations is the transmitter and the others are the receivers. In summary, the shape of the signals did not change, and they were different only in the signal amplitude and the shift that occurred when they faced the breast model.

The antenna (A1) transmits a UWB pulse, while other sensors receive the signal. Figure 15 shows a graph of received signals from five different sensors (A2, A5, A8, A10, and A12) when a tumor exists inside the breast. It shows that the signals were shifted down when the tumor exists. In the simulation, antenna arrays were placed at different positions to show how the distance and angle could affect signal reception (Fig. 14). Besides, signals arriving at receivers are delayed, which shift signal peaks. Thus, signals have the same shape but with changes in the amplitude that are specific for each array position. Therefore, it is useful to apply a fidelity factor (FF) to show signal similarity and low distortion. The result in Fig. 16 shows more

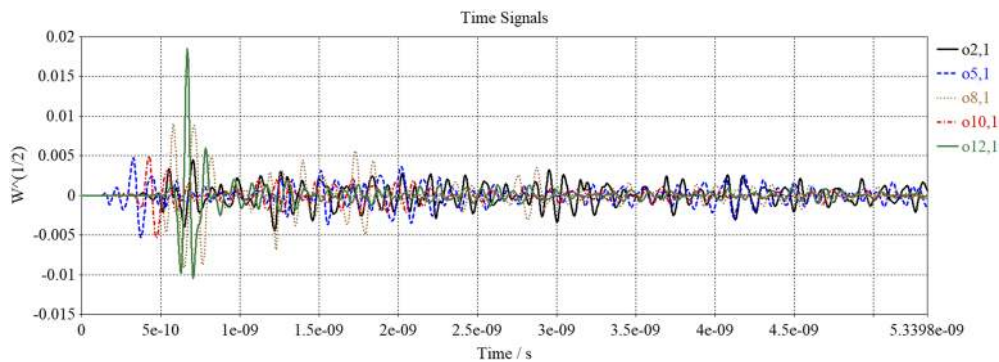


FIG. 15. The recipient signals from different arrays of the antenna on the breast model.

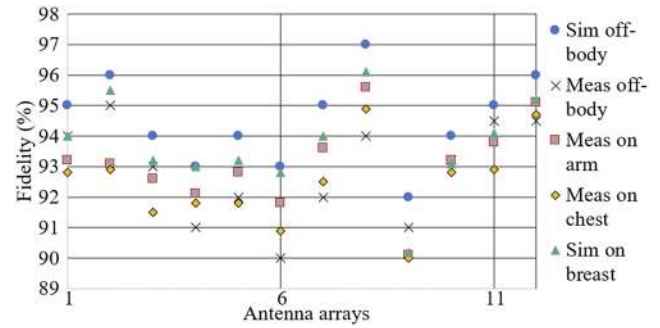


FIG. 16. Fidelity percentage of the recipient signals for off-body, on arm, and on chest and simulation on the breast.

than 90% similarity in FFs for the simulated samples. The following equations below show the fidelity formula:

$$F = \max \int_{-\infty}^{+\infty} \hat{x}(t) \cdot \hat{y}(t - \tau) dt$$

where

$$\hat{x}(t) = \frac{x(t)}{\sqrt{\int_{-\infty}^{+\infty} |x(t)|^2 dt}}, \text{ and } \hat{y}(t) = \frac{y(t)}{\sqrt{\int_{-\infty}^{+\infty} |y(t)|^2 dt}} \quad (1)$$

where τ is the shifted time and F is assumed as the maximum cross correlation function of two signals when they have normalized to their level energy. The fidelity value varies between $0 \leq F \leq 1$, where zero indicates that there is no similarity between the two signals, and one shows that both signals are 100% similar.⁶⁵

Apart from the fidelity factor, the mutual coupling among antenna arrays is another vital parameter in imaging. The mutual coupling results of the antenna arrays around the breast are shown in Fig. 17. They depict a very good mutual coupling and isolation among the antenna arrays since the transmission coefficient level of the antenna arrays is less than -20 dB at most of its operating bandwidth.

B. Image reconstruction of tumor in breast

All the recipient signals shown in Fig. 15 are extracted and analyzed from CST and imported to MATLAB to reconstruct the image of the breast tumor sample using the simulation data at a

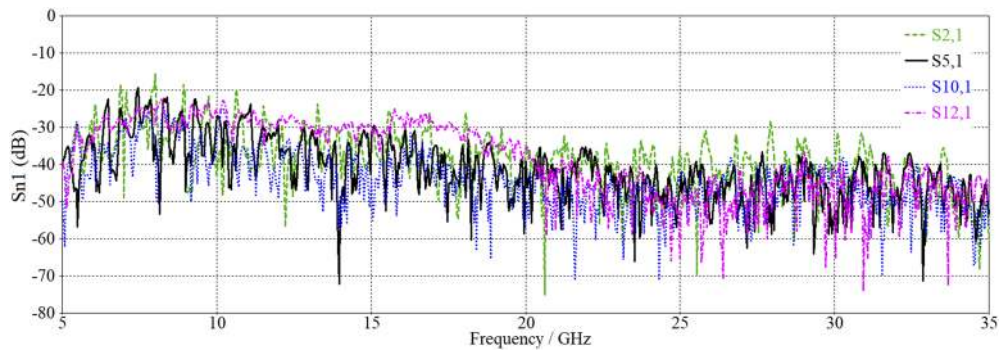


FIG. 17. The transmission coefficient results from four arrays on the body.

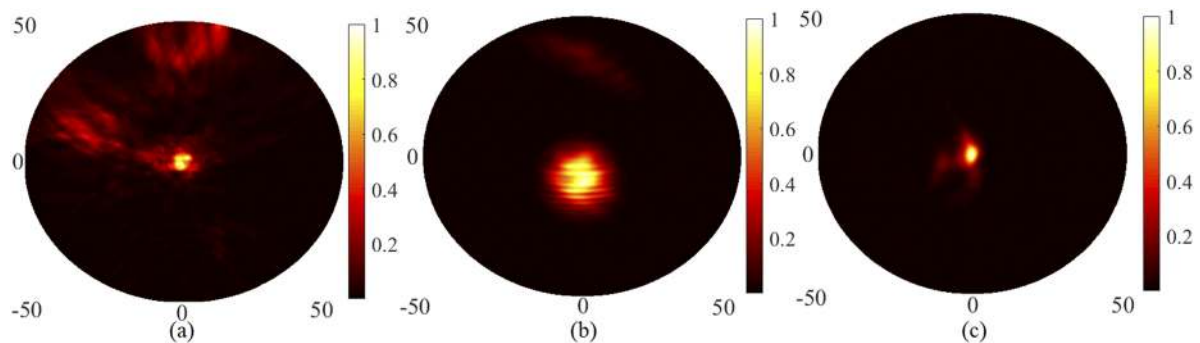


FIG. 18. The reconstructed image of breast tumor using the robust time-reversal algorithm using (a) 4 arrays, (b) 8 arrays, and (c) 12 arrays.

diameter of 4 mm. The robust time-reversal algorithm presented in Ref. 66 was being used to reconstruct the image using several considerations such as array numbers around a tumor, different locations of two tumors, and larger breast size samples. Figure 18 indicates the image reconstruction of the tumor located at the center of the breast size with a diameter of 50 mm for different antenna arrays of 4, 8, and 12. The results discovered that the UWB antenna system can detect a tumor with a diameter of 4 mm. Since the working BW of the antenna is about 29 GHz, the range resolution of the antenna is about 5 mm using the equation presented in Refs. 67–69. Thus, the 4 mm diameter of tumor was chosen for our investigation to show if the antenna arrays can detect a target smaller than that size. The reconstructed image is, however, clearest when the antenna arrays

are 12 where the clutters and artifacts caused by the skin layers and the other arrays were perfectly removed.

To evaluate the UWB antenna system capability in image reconstruction, two tumors, one at the center and the other off-center, are located within the breast. The robust time-reversal algorithm is used to reconstruct the image. Figure 19 depicts that both tumors were properly detected. However, some negligible clutters are existing.

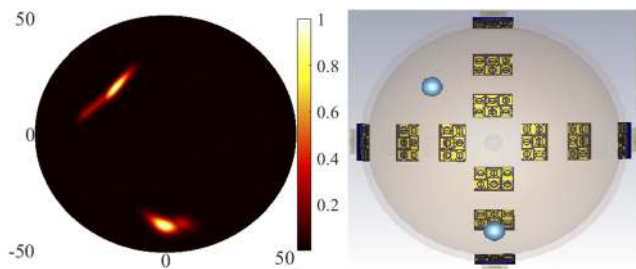


FIG. 19. The reconstruction image of two tumors in the breast.

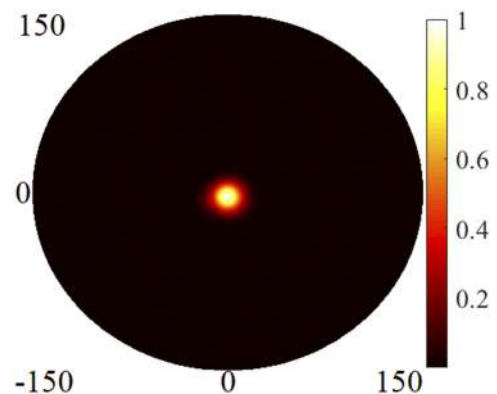


FIG. 20. Image reconstruction of the breast sample with dimensions of 150 mm.

Another factor that should be evaluated is to investigate if the antenna system can detect the same small tumor with a diameter of 4 mm in the bigger breast sample. Thus, a breast size with a diameter of 150 mm was considered for the imaging environment in the simulation. Figure 20 shows that the antenna system can detect and localize the tumor even within a larger breast sample.

IV. CONCLUSION

A metamaterial-based wearable flexible UWB antenna is designed at 5G frequency bands for breast cancer imaging and WBAN applications. It is integrated with six MTM arrays, where the MTM unit cell consists of an SRR with a modified rice grain shape, and two CLSs. Afterward, the characteristics of the MTM unit cell such as permittivity, permeability, and refraction index were extracted and calculated. Optimized parameters indicated in the simulation guided the capability of the fabricated prototype for measurement such as removing the stop bands and expanding BW by integrating six arrays of the MTM unit cell with the antenna to enhance the BW, gain, radiation efficiency, and directivity. The results exhibit good agreement between the simulation and measurement results on both the arm and the chest with the SAR values less than 2 W/kg for both standards of 1 g and 10 g. The antenna yielded the results of more than 70% for radiation efficiency and maximum directional gain of 8.85 dB over its operating frequency band. Then, the performance of the antenna was evaluated for both on-body and off-body cases. The proposed antenna array system promisingly offers the capability to detect a tumor with a diameter of 4 mm in any location inside the breast, even for two tumors and a larger breast size. Conclusively, the proposed wearable flexible metamaterial based UWB antenna system is a proven suitable method and economical for the applications of both WBAN and breast imaging.

ACKNOWLEDGMENTS

The authors express their gratitude to the Ministry of Education and the deanship of scientific research—Najran University—Kingdom of Saudi Arabia for their financial and technical support under Code No. (NU/ESCI/17/034).

REFERENCES

- See <https://www.cdc.gov/coronavirus/2019-ncov/hcp/telehealth.html> for using Telehealth to Expand Access to Essential Health Services during the COVID-19 Pandemic.
- W. Wang, X. W. Xuan, P. Pan, Y. J. Hua, H. B. Zhao, and K. Li, "A low-profile dual-band omnidirectional Alford antenna for wearable WBAN applications," *Microwave Opt. Technol. Lett.* **62**(5), 2040–2046 (2020).
- R. S. Dilmaghani, H. Bobarshad, M. Ghavami, S. Choobkar, and C. Wolfe, "Wireless sensor networks for monitoring physiological signals of multiple patients," *IEEE Trans. Biomed. Circuits Syst.* **5**(4), 347–356 (2011).
- T.-W. Koo, Y.-J. Hong, G.-k. Park, K. Shin, and J.-G. Yook, "Extremely low-profile antenna for attachable bio-sensors," *IEEE Trans. Antennas Propag.* **63**(4), 1537–1545 (2015).
- Q. H. Abbasi, A. Sani, A. Alomainy, and Y. Hao, "Arm movements effect on ultra wideband on-body propagation channels and radio systems," in *Loughborough Antennas and Propagation Conference, LAPC 2009—Conference Proceedings* (IEEE, 2009), pp. 261–264.
- Q. H. Abbasi, M. M. Khan, S. Liaqat, M. Kamran, A. Alomainy, and Y. Hao, "Experimental investigation of ultra wide-band diversity techniques for on-body radio communications," *Prog. Electromagn. Res. C* **34**, 165–181 (2012).
- Q. H. Abbasi, H. El Sallabi, N. Chopra, K. Yang, K. A. Qaraqe, and A. Alomainy, "Terahertz channel characterization inside the human skin for nano-scale body-centric networks," *IEEE Trans. Terahertz Sci. Technol.* **6**(3), 427–434 (2016).
- K. N. Paracha, S. K. Abdul Rahim, P. J. Soh, and M. Khalily, "Wearable antennas: A review of materials, structures, and innovative features for autonomous communication and sensing," *IEEE Access* **7**, 56694–56712 (2019).
- Q. H. Abbasi, M. Ur Rehman, K. Qaraqe, and A. Alomainy, "Advances in body-centric wireless communication: Applications and state-of-the-art," in *Advances in Body-Centric Wireless Communication: Applications and State-of-the-Art* (The Institution of Engineering and Technology (IET), 2016), pp. 1–438.
- M. M. Khan, Y. Hao, Q. H. Abbasi, C. Parini, and A. Alomainy, "Experimental characterisation of ultra-wideband off-body radio channels considering antenna effects," *IET Microwaves, Antennas Propag.* **7**(5), 370–380 (2013).
- M. N. Sudha and S. J. Benitta, "Design of antenna in wireless body area network (WBAN) for biotelemetry applications," *Intell. Decis. Technol.* **10**(4), 365–371 (2016).
- D. Mandal and S. S. Pattnaik, "Quad-band wearable slot antenna with low SAR values for 1.8 GHz DCS, 2.4 GHz WLAN and 3.6/5.5GHz WiMAX applications," *Prog. Electromagn. Res. B* **81**, 163–182 (2018).
- M. Ur-Rehman, N. A. Malik, X. Yang, Q. H. Abbasi, Z. Zhang, and N. Zhao, "A low profile antenna for millimeter-wave body-centric applications," *IEEE Trans. Antennas Propag.* **65**(12), 6329–6337 (2017).
- A. Alemaryeen and S. Noghianian, "Crumpling effects and specific absorption rates of flexible AMC integrated antennas," *IET Microwaves, Antennas Propag.* **12**(4), 627–635 (2018).
- A. Alomainy, R. Di Bari, Q. H. Abbasi, and Y. Chen, "Antenna design requirements for wireless BAN and WSNs," in *Co-Operative and Energy Efficient Body Area and Wireless Sensor Networks for Healthcare Applications* (Academic Press, Science Direct, 2014), pp. 7–23.
- P. J. Soh *et al.*, "A smart wearable textile array system for biomedical telemetry applications," *IEEE Trans. Microwave Theory Tech.* **61**(5), 2253–2261 (2013).
- R. Yahya, M. R. Kamarudin, and N. Seman, "Effect of rainwater and seawater on the permittivity of denim jean substrate and performance of UWB eye-shaped antenna," *IEEE Antennas Wireless Propag. Lett.* **13**, 806–809 (2014).
- D. L. Paul, H. Giddens, M. G. Paterson, G. S. Hilton, and J. P. McGeehan, "Impact of body and clothing on a wearable textile dual band antenna at digital television and wireless communications bands," *IEEE Trans. Antennas Propag.* **61**(4), 2188–2194 (2013).
- Q. Bai and R. Langley, "Wearable EBG antenna bending and crumpling," in *Loughborough Antennas and Propagation Conference, LAPC 2009—Conference Proceedings* (IEEE, 2009), pp. 201–204.
- A. Y. I. Ashyap *et al.*, "Compact and low-profile textile EBG-based antenna for wearable medical applications," *IEEE Antennas Wireless Propag. Lett.* **16**, 2550–2553 (2017).
- S. Yan and G. A. E. Vandenbosch, "Radiation pattern-reconfigurable wearable antenna based on metamaterial structure," *IEEE Antennas Wireless Propag. Lett.* **15**, 1715–1718 (2016).
- E. F. Sundarsingh, S. Velan, M. Kanagasabai, A. K. Sarma, C. Raviteja, and M. G. N. Alsath, "Polygon-shaped slotted dual-band antenna for wearable applications," *IEEE Antennas Wireless Propag. Lett.* **13**, 611–614 (2014).
- R. B. V. B. Simorangkir, Y. Yang, L. Matekovits, and K. P. Esselle, "Dual-band dual-mode textile antenna on PDMS substrate for body-centric communications," *IEEE Antennas Wireless Propag. Lett.* **16**, 677–680 (2017).
- J. G. Andrews, S. Buzzi, W. Choi, S. V. Hanly, A. Lozano, A. C. K. Soong, and J. C. Zhang, "What will 5G be?," *IEEE J. Sel. Areas Commun.* **32**, 1065–1082 (2014).
- F. Tariq, M. R. A. Khandaker, K.-K. Wong, M. Imran, and M. Bennis, "A speculative study on 6G," in *IEEE Magazine* (IEEE, 2019).
- S. V. Hum and J. Perruisseau-Carrier, "Reconfigurable reflectarrays and array lenses for dynamic antenna beam control: A review," *IEEE Trans. Antennas Propag.* **62**, 183–198 (2014).
- C. Borda-Fortuny, K.-F. Tong, A. Al-Armaghany, and K.-K. Wong, "A low-cost fluid switch for frequency-reconfigurable Vivaldi antenna," *IEEE Antennas Wireless Propag. Lett.* **16**, 3151–3154 (2017).

- ²⁸S. Chinchali *et al.*, "Network offloading policies for cloud robotics: A learning-based approach," in *Robotics: Science and Systems 2019* (Freiburg im Breisgau, Germany, 2019), pp. 1–10.
- ²⁹M. Chen *et al.*, "Cognitive internet of vehicles," *Comput. Commun.* **120**, 58–70 (2018).
- ³⁰X.-F. Teng, Y.-T. Zhang, C. C. Poon, and P. Bonato, "Wearable medical systems for p-health," *IEEE Rev. Biomed. Eng.* **1**, 62–74 (2008).
- ³¹M. J. W. Rodwell, Y. Fang, J. Rode, J. Wu, B. Markman, S. T. uran Brunelli, J. Klamkin, and M. Urteaga, "100–340 GHz systems: Transistors and applications," in *2018 IEEE International Electron Devices Meeting (IEDM)* (IEEE, 2018), pp. 14.3.1–14.3.4.
- ³²M. Aladsani, A. Alkhateeb, and G. C. Trichopoulos, "Leveraging mmwave imaging and communications for simultaneous localization and mapping," in *International Conference on Acoustics, Speech, and Signal Processing (ICASSP)* (IEEE, 2019), pp. 1–4.
- ³³T. S. Rappaport, "6G and beyond: Terahertz communications and sensing," in *2019 Brooklyn 5G Summit Keynote* (IEEE.tv, 2019); available at <https://ieeetv.ieee.org/conference-highlights/keynote-ted-rappaport-terahertz-communication-b5gs-2019/>
- ³⁴P. C. Jain, "Wireless body area network for medical healthcare," *IETE Tech. Rev.* **28**(4), 362 (2011).
- ³⁵L. Zheng, J. Yang, H. Cai, W. Zhang, J. Wang, and Y. Yu, "MAGENT: A many-agent reinforcement learning platform for artificial collective intelligence," in *Proceedings of the 32nd AAAI Conference on Artificial Intelligence. AI (AAAI-18)* (The Association for the Advancement of Artificial Intelligence, 2018).
- ³⁶N. Hussain and I. Park, "Design of a wide-gain-bandwidth metasurface antenna at terahertz frequency," *AIP Adv.* **7**, 055313 (2017).
- ³⁷S. Chaimool, T. Hongnara, C. Raklua, P. Akkraekthalin, and Y. Zhao, "Design of a PIN diode-based reconfigurable metasurface antenna for beam switching applications," *Int. J. Antennas Propag.* **2019**, 7216324 ().
- ³⁸P. Dawar, N. S. Raghava, and A. De, "UWB metamaterial-loaded antenna for C-band Applications," *Int. J. Antennas Propag.* **2019**, 6087039.
- ³⁹J. Eichenberger, E. Yetisir, and N. Ghalichechian, "High gain antipodal UWB vivaldi antenna with pseudoelement and notched tapered slot operating at 2.5–57 GHz," *IEEE Trans. Antennas Propag.* **67**(7), 4357 (2019).
- ⁴⁰M. El Gharbi, M. Martinez-Estrada, R. Fernández-García, S. Ahyoud, and I. Gil, "A novel ultra-wide band wearable antenna under different bending conditions for electronic-textile applications," *J. Text. Inst.* **2020**, 1–7.
- ⁴¹S. Doddipalli, A. Kothari, and P. Peshwe, "A low profile ultrawide band monopole antenna for wearable applications," *Int. J. Antennas Propag.* **2017**, 7362431 (2017).
- ⁴²M. Koohestani, N. Pires, A. K. Skrivervik, and A. A. Moreira, "Bandwidth enhancement of a wearable UWB antenna near a human arm," *Microwave Technol. Lett.* **55**(12), 2965 (2013).
- ⁴³C.-Y.-D. Sim, C.-W. Tseng, and H.-J. Leu, "Embroidered wearable antenna for ultrawideband applications," *Microwave Technol. Lett.* **54**(11), 2597 (2012).
- ⁴⁴M. Karimyian-Mohammadabadi, M. A. Dorostkar, F. Shokuohi, M. Shanbeh, and A. Torkan, "Super-wideband textile fractal antenna for wireless body area networks," *J. Electromagn. Waves Appl.* **29**(13), 1728 (2015).
- ⁴⁵A. Anbalagan, E. F. Sundarsingh, V. S. Ramalingam, A. Samdaria, D. B. Gurion, and K. Balamurugan, "Realization and analysis of a novel low-profile embroidered textile antenna for real-time pulse monitoring," *IETE J. Res.* **2020**, 1–8.
- ⁴⁶V. Aruna, M. G. N. Alsath, S. Kirubaveni, and M. Maheswari, "Flexible and beam steerable planar UWB Quasi-Yagi antenna for WBAN," *IETE J. Res.* **2019**, 1–11.
- ⁴⁷P. M. Potey and K. Tuckley, "Design of wearable textile antenna for low back radiation," *J. Electromagn. Waves Appl.* **34**(2), 235 (2020).
- ⁴⁸H. A. Shaban, M. A. El-Nasr, and R. M. Buehrer, "Localization with sub-millimeter accuracy for UWB-based wearable human movement," *J. Electromagn. Waves Appl.* **25**, 11–12 (2011).
- ⁴⁹P. Kumar Rao and R. Mishra, "Elliptical shape flexible MIMO antenna with high isolation for breast cancer detection application," *IETE J. Res.* (published online).
- ⁵⁰R. Garg, P. Bhartia, I. Bahl, and A. Ittipiboon, *Microstrip Antenna Design Handbook* (Artech House, Inc., 2001).
- ⁵¹M. M. Islam, M. T. Islam, M. Samsuzzaman, and M. R. I. Faruque, "Compact metamaterial antenna for UWB applications," *Electron. Lett.* **51**(16), 1222–1224 (2015).
- ⁵²M. Faenzi, G. Minatti, D. González-Ovejero, F. Caminita, E. Martini, C. Della Giovampaola, and S. Maci, "Metasurface antennas: New models, applications and realizations," *Sci. Rep.* **10**, 10178 (2019).
- ⁵³D. R. Smith, W. J. Padilla, D. Vier, S. C. Nemat-Nasser, and S. Schultz, "Composite medium with simultaneously negative permeability and permittivity," *Phys. Rev. Lett.* **84**(18), 4184 (2000).
- ⁵⁴Y. Dong, H. Toyao, and T. Itoh, "Design and characterization of miniaturized patch antennas loaded with complementary split-ring resonators," *IEEE Trans. Antennas Propag.* **60**(2), 772–785 (2012).
- ⁵⁵Z. Mousavi Razi and P. Rezaei, "Fabry perot cavity antenna based on capacitive loaded strips superstrate for X-band satellite communication," *ARS J.* **2**(1), 26–30 (2013).
- ⁵⁶E. J. Rothwell, J. L. Frasca, S. M. Ellison, P. Chahal, and R. O. Ouedraogo, "Analysis of the nicolson-ross-weir method for characterizing the electromagnetic properties of engineered materials," *Prog. Electromagn. Res.* **157**, 31–47 (2016).
- ⁵⁷M. Hamza and W. T. Khan, "Hybrid utilization of loading techniques and cavity groove for performance enhancement of the UWB (2–18 GHz) spiral antenna," *Int. J. Antennas Propag.* **2018**, 9167154.
- ⁵⁸C. Ballesteros, A. Pfadler, J. Romeu, and L. Jofre, "5G vehicle MIMO antenna capacity based on a rigorous electromagnetic channel modeling," in *48th European Microwave Conference (EuMC)*, September 2018.
- ⁵⁹S. F. Jilani, Q. H. Abbasi, and A. Alomainy, "Inkjet-printed millimetre-wave PET-based flexible antenna for 5G wireless applications," in *2018 IEEE MTT-S International Microwave Workshop Series on 5G Hardware and System Technologies (IMWS-5G)*, August 2018.
- ⁶⁰H. A. E. Elobaid, S. Kamal, A. Rahim, M. Himdi, X. Castel, and M. A. Kasgari, "A transparent and flexible polymer-fabric tissue UWB antenna for future wireless networks," *IEEE Antennas Wireless Propag. Lett.* **16**, 1333 (2017).
- ⁶¹W. Li, A. Meredov, and Atif Shamim, "Silver nanowire based flexible, transparent, wideband antenna for 5G band Application," in *2019 IEEE International Symposium on Antennas and Propagation and UNSC-URSI Radio Science Meeting*, October 2019.
- ⁶²B. Biswas, R. Ghatak, and D. R. Poddar, "A fern fractal leaf inspired wideband Antipodal vivaldi antenna for microwave imaging system," *IEEE Trans. Antennas Propag.* **65**(11), 6126 (2017).
- ⁶³P. A. J. Kolarsick, M. A. Kolarsick, and C. Goodwin, "Anatomy and physiology of the skin," *J. Dermatol. Nurses Assoc.* **3**(4), 203–213 (2011).
- ⁶⁴See https://www.healthline.com/health/stratum-corneum#_noHeaderPrefixedContent for What Is the Stratum Corneum?: Function.
- ⁶⁵T. Saeidi, I. Ismail, R. Adam, H. Alhawari, and W. P. Wen, "Near-field and far-field investigation of miniaturized UWB antenna for imaging of wood," *AIP Adv.* **9**, 035232 (2019).
- ⁶⁶T. Saeidi, I. Ismail, S. N. Mahmood, S. Alani, and A. R. H. Alhawari, "Microwave imaging of voids in oil palm trunk applying UWB antenna and robust time-reversal algorithm," *J. Sens.* **2020**, 8895737.
- ⁶⁷H.-J. Li, T.-Y. Liu, and S.-H. Yang, "Superhigh image resolution for microwave imaging," *Int. J. Imaging Technol.* **2**(1), 37–46 (1990).
- ⁶⁸N. Simonov, S.-H. Son, B.-R. Kim, and S.-I. Jeon, "Investigation of spatial resolution in a microwave tomography system," in *2014 International Conference on Electronics, Information and Communications (ICEIC)* (Kota Kinabalu, Malaysia, 2014), pp. 305–700.
- ⁶⁹N. A. Simonov, S. I. Jeon, S. H. Son, J. M. Lee, and H. J. Kim, *About Equivalency of Two Methods of Information Gathering in Microwave Imaging* (Radio Technology Research Department, ETRI, Daejeon, South Korea, 2012).